Shallow-crustal metamorphism during Late Cretaceous anatexis in the Sevier hinterland plateau: Peak temperature conditions from the Grant Range, eastern Nevada, U.S.A.

Sean P. Long[1]*, Emmanuel Soignard[2]
[1]SCHOOL OF THE ENVIRONMENT, WASHINGTON STATE UNIVERSITY, PULLMAN, WASHINGTON 99164, USA
[2]LEROY EYRING CENTER FOR SOLID STATE SCIENCE, ARIZONA STATE UNIVERSITY, TEMPE, ARIZONA 85287, USA

ABSTRACT

Documenting spatio-temporal relationships between the thermal and deformation histories of orogenic systems can elucidate their evolution. In the Sevier hinterland plateau in eastern Nevada, an episode of Late Cretaceous magmatism and metamorphism affected mid- and upper-crustal levels, concurrent with late-stage shortening in the Sevier thrust belt. Here, we present quantitative peak temperature data from the Grant Range, a site of localized, Late Cretaceous granitic magmatism and greenschist facies metamorphism. Twenty-two samples of Cambrian to Pennsylvanian metasedimentary and sedimentary rocks were analyzed, utilizing Raman spectroscopy on carbonaceous material, vitrinite reflectance, and Rock-Eval pyrolysis thermometry. A published reconstruction of Cenozoic extension indicates that the samples span pre-extensional depths of 2.5–9 km. Peak temperatures systematically increase with depth, from ~100 to 300 °C between 2.5 and 4.5 km, ~400 to 500 °C between 5 and 8 km, and ~550 °C at 9 km. The data define a metamorphic field gradient of ~60 °C/km, and are corroborated by quartz recrystallization microstructure and published conodont alteration indices.

Metamorphism in the Grant Range is correlated with contemporary, upper-crustal metamorphism and magmatism documented farther east in Nevada, where metamorphic field gradients as high as ~50 °C/km are estimated. These data have implications for localized but significant thermal weakening of the plateau crust, including attaining temperatures for quartz plasticity at depths of ~5–6 km, and the potential for partial melting possibly as shallow as ~12–15 km. Thermal weakening may have contributed to a slowing of shortening rates documented in the Sevier thrust belt at this latitude at ca. 88 Ma, by locally inducing mid- and lower-crustal ductile thickening in the hinterland.

LITHOSPHERE; v. 8; no. 2; p. 150–164; GSA Data Repository Item 2016051 | Published online 25 January 2016 doi: 10.1130/L501.1

INTRODUCTION

Understanding the thermal history of an orogenic belt, and its relationship in space and time to the corresponding deformation history, can provide critical insights into the evolution of orogenic systems. In the Jurassic-Paleogene U.S. Cordilleran orogenic belt, an episode of Late Cretaceous (ca. 70–90 Ma) granitic magmatism and accompanying metamorphism has been documented in the hinterland plateau of the Sevier thrust belt in eastern Nevada and western Utah (e.g., Miller et al., 1988; Barton, 1990), which produced greenschist and amphibolite facies metasedimentary rocks that are now exposed within a series of highly extended ranges (Fig. 1). However, the complex overprint of Cenozoic extension across Nevada and Utah in many places hinders placing these rocks in an accurate pre-extensional structural and depth context, in particular for greenschist facies rocks that do not contain the mineral assemblages necessary for quantitative thermobarometry. This, combined with a wealth of studies that have focused on determining the pressure and temperature conditions of upper amphibolite facies rocks exhumed in the footwalls of core complexes (e.g., McGrew et al., 2000; Cooper et al., 2010; Wells et al., 2012; Hallett and Spear, 2014), has led to a prevailing view that metamorphism in the Sevier hinterland dominantly affected mid-crustal levels, despite earlier efforts that presented field relations emphasizing that high temperatures were locally attained in the upper crust (Miller et al., 1988; Miller and Gans, 1989).

Part of the difficulty of determining the conditions of shallow-crustal metamorphism is that, until recently, quantitative techniques for analyzing the peak temperature of sub-garnet grade rocks have not been available. Thermal maturation parameters utilized in the petroleum industry, such as vitrinite reflectance, can estimate the peak temperature of sedimentary rocks within ±20–30 °C, but are applicable only up to peak temperatures of ~200–300 °C (e.g., Mukhopadhyay, 1994). Semiquantitative peak temperature parameters, such as conodont alteration index, only yield broad (~200 °C) bracketing ranges for metasedimentary rocks that experienced peak temperatures ≥300 °C (Königshof, 2003). However, with the development of Raman spectroscopy on carbonaceous material (RSCM) thermometry (Beyssac et al., 2002), peak temperatures for greenschist facies metasedimentary rocks that contain organic matter can be determined within ±50 °C. This technique is ideal for understanding the thermal conditions of thick sedimentary sections such as the Cordilleran passive margin basin in eastern Nevada, which is dominated by organic-rich carbonates (e.g., Stewart, 1980).

In this study, we present quantitative peak temperature determinations from Paleozoic sedimentary and metasedimentary rocks in the Grant Range in eastern Nevada, which represents the westernmost of a series of exposures of Late Cretaceous metamorphic rocks in the Sevier hinterland in eastern Nevada (Figs. 1, 2). The samples are placed in a detailed structural

*sean.p.long@wsu.edu

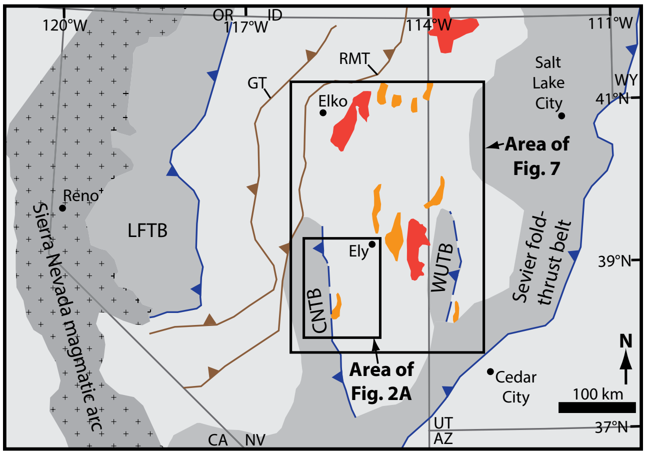

Figure 1. Map of Cordilleran retroarc region in Nevada (NV), Utah (UT), and California (CA) (modified from Long, 2015). Deformation fronts of Cordilleran thrust systems shown in blue, with spatial extents shaded gray. Late Paleozoic thrust systems shown in brown. Areas of exposed Jurassic and Cretaceous metamorphic rocks are highlighted, including metamorphic core complexes in red and highly extended ranges in orange. AZ—Arizona; CNTB—Central Nevada thrust belt; GT—Golconda thrust; ID—Idaho; LFTB—Luning-Fencemaker thrust belt; OR—Oregon; RMT—Roberts Mountains thrust; WUTB—Western Utah thrust belt; WY—Wyoming.

context, obtained from a recently published structural reconstruction of the Grant Range (Long and Walker, 2015), which shows that they were distributed between crustal depths of ~2.5–9 km prior to Cenozoic extension. Three different thermometry techniques are utilized, including RSCM on Cambrian, Ordovician, and Silurian rocks, and vitrinite reflectance and Rock-Eval pyrolysis on Devonian, Mississippian, and Pennsylvanian rocks. The temperature data are used to quantify a metamorphic field gradient, which is interpreted to reflect the peak thermal conditions for Late Cretaceous metamorphism in the Grant Range. We then compare this data to other studied areas of Late Cretaceous, shallow-crustal metamorphism in eastern Nevada, and discuss implications for localized thermal weakening of the Sevier hinterland plateau crust during the late stages of Cordilleran orogenesis.

CORDILLERAN TECTONIC FRAMEWORK OF EASTERN NEVADA

From the Neoproterozoic to the Triassic, >10 km of shallow-marine sedimentary rocks were deposited on the western Laurentian continental shelf in eastern Nevada (e.g., Stewart, 1980). During the Jurassic, establishment of an Andean-style subduction system on the western North American plate margin initiated construction of the Cordilleran orogenic belt, which continued until the Paleogene (e.g., DeCelles, 2004). For the duration of orogenesis, eastern Nevada was situated within a broad hinterland region between the Sierra Nevada magmatic arc and the Sevier fold-thrust belt, the locus of upper-crustal shortening (Fig. 1). The timing of the initiation of shortening in the Sevier thrust belt is debated; most agree that the onset of Early Cretaceous (ca. 130 Ma) foreland basin subsidence indicates the onset of shortening (e.g., Jordan, 1981; Currie, 2002), while some argue for emplacement of thrust sheets as early as the latest Jurassic (ca. 145 Ma) (e.g., DeCelles and Coogan, 2006). The onset of crustal thickening in parts of the Sevier hinterland is interpreted to have begun as early as the Late Jurassic (ca. 150 Ma), on the basis of initial prograde metamorphism recorded within rocks now exhumed in the footwalls of metamorphic core complexes (Hoisch et al., 2014; Cruz-Uribe et al., 2015; Kelly et al., 2015) and isotopic compositions of Late Jurassic plutons (Chapman et al., 2015).

In Nevada, low-magnitude (a few 10s of km) upper-crustal shortening of likely Cretaceous age was accommodated in the Central Nevada thrust belt (Taylor et al., 2000; Long, 2012; Long et al., 2014) and by regional-scale, open folding across much of eastern Nevada (Long, 2015). However, thermobarometry of exhumed mid-crustal rocks indicates localized but significant Cretaceous crustal thickening, including within the Snake Range core complex in east-central Nevada (e.g., Lewis et al., 1999; Cooper et al., 2010), the Ruby–East Humboldt core complex in northeast Nevada (e.g., Hodges and Walker, 1992; McGrew et al., 2000; Hallett and Spear, 2014), and in the footwall of the Windermere thrust in northeast Nevada (Camilleri and Chamberlain, 1997). By the Late Cretaceous, near the end of crustal thickening, the Sevier hinterland is interpreted to have been a high-elevation orogenic plateau (e.g., Coney and Harms, 1984; DeCelles, 2004), named the "Nevadaplano" after comparison to the Andean Altiplano. The Nevadaplano was underlain by crust that was locally as thick as ~50–60 km (Coney and Harms, 1984; Gans, 1987; DeCelles and Coogan, 2006; Colgan and Henry, 2009; Chapman et al., 2015), which supported surface elevations as high as ~3 km (Cassel et al., 2014; Snell et al., 2014).

During Cordilleran orogenesis, two episodes of granitic magmatism, one in the Jurassic (ca. 155–165 Ma) and one in the Late Cretaceous (ca. 70–90 Ma), have been documented in eastern Nevada and western Utah, and each is associated spatially and temporally with metamorphism and ductile, contractional deformation (e.g., Barton et al., 1988; Miller et al., 1988; Miller and Hoisch, 1995; Wells and Hoisch, 2008). The Jurassic episode, which in most places is characterized by spatially localized metamorphism in proximity to upper-crustal intrusions (Miller et al., 1988; Miller and Hoisch, 1995), has been interpreted as heating and low-magnitude contractional deformation that accompanied a pulse of back-arc magmatism (Miller and Hoisch, 1995). The more regionally significant Late Cretaceous magmatic event produced the peak metamorphic conditions recorded in much of eastern Nevada (Miller and Gans, 1989; Barton, 1990), and affected both mid- and upper-crustal levels. This event occurred late during the Sevier shortening history, while the Nevadaplano was approaching its maximum crustal thickness (e.g., DeCelles and Coogan, 2006), and was locally associated with significant crustal thickening (Camilleri and Chamberlain, 1997; McGrew et al., 2000). Late Cretaceous magmatism has been interpreted as the shallow thermal expression of lower-crustal anataxis, which was initiated as a result of eastward migration of subduction-related magmatism coupled with conductive relaxation of isotherms within structurally thickened crust (Miller and Gans, 1989), or alternatively, as a result of heat influx following delamination of dense mantle lithosphere (Wells and Hoisch, 2008; Wells et al., 2012).

During the Late Cretaceous and Paleocene (ca. 80–60 Ma), spatially isolated extension is recorded in the Nevadaplano, during the final stages of shortening in the Sevier thrust belt (Hodges and Walker, 1992; Camilleri and Chamberlain, 1997; Wells and Hoisch, 2008; Druschke et al., 2009; Long et al., 2015), and has been interpreted as a consequence of thermal weakening and isostatic adjustment following lithospheric delamination (Wells and Hoisch, 2008). In addition, spatially isolated, post-orogenic, Eocene-Oligocene extension has been documented in eastern Nevada (e.g., Gans et al., 2001; Druschke et al., 2009; Long and Walker, 2015), and was often associated in space and time with the sweep of silicic volcanism that accompanied post-Laramide slab rollback (Humphreys, 1995; Dickinson, 2002). The inception of widespread extension that formed

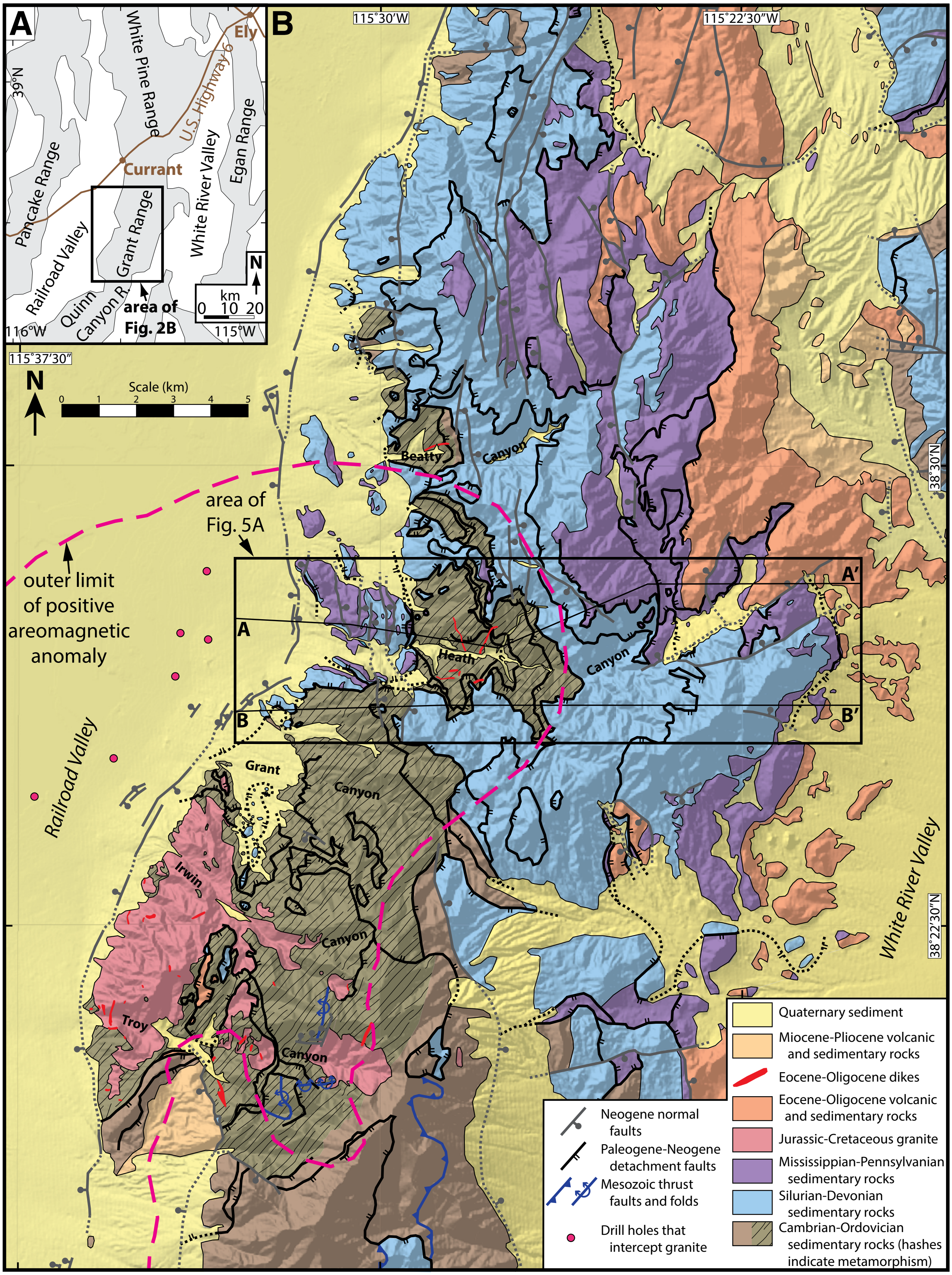

Figure 2. (A) Map showing location of the Grant Range and geographic names of surrounding ranges and valleys. (B) Generalized geologic map of the Grant Range, modified from Long and Walker (2015). Compiled source maps include Moores et al. (1968), Kleinhampl and Ziony (1985), Lund et al. (1987; 1988), Fryxell (1988), Camilleri (2013), and Long (2014). Dashed pink line shows outer limit of positive aeromagnetic anomaly interpreted to delineate subsurface extent of Troy pluton (Lund et al., 1987, 1988; Blank, 1993). Locations of Railroad Valley drill holes that intercept granite at depth are from Hess et al. (2004).

the Basin and Range province, and accompanying lowering of the surface elevation of the Nevadaplano, was not until the middle Miocene (e.g., Dickinson, 2002; Colgan and Henry, 2009; Cassel et al., 2014).

DEFORMATION, METAMORPHISM, AND MAGMATISM IN THE GRANT RANGE

An 8-km-thick section of Cambrian-Pennsylvanian sedimentary rocks is exposed in the Grant Range (Figs. 2, 3), and is dominated by carbonates (Fryxell, 1988; Lund et al., 1993; Camilleri, 2013; Long and Walker, 2015). Cambrian and Ordovician rocks have experienced greenschist facies metamorphism and low-magnitude, penetrative contractional strain (Figs. 4B, 4D), both of which die out upsection, and are not observed in Silurian-Pennsylvanian rocks (Fryxell, 1988; Lund et al., 1993; Camilleri, 2013). Readers are referred to Camilleri (2013) for detailed descriptions of micro- and mesoscale ductile structures and metamorphic lithologies, textures, and mineral assemblages in the study area in the central Grant Range (Fig. 2). Rock unit divisions discussed below and shown on Figure 3 are after Long and Walker (2015). Cambrian and Ordovician sandy and silty limestone protoliths have been metamorphosed to recrystallized limestone with abundant mica porphyroblasts, with silty partings metamorphosed to argillite and phyllite (Figs. 4A, 4C), and more pure limestone protoliths have been metamorphosed to crystalline marble (Figs. 4B, 4D). Moving downsection through the stratigraphic column (Fig. 3), sericite (defined here as fine-grained white mica) and chlorite first appear within upper Ordovician rock units, tourmaline and white mica porphyroblasts appear at the top of the Cambrian section, and phlogopite, amphibole (Fig. 4C), and biotite porphyroblasts are observed within the lowest Cambrian units in the study area (Camilleri, 2013). All metasedimentary rock units observed in the study area have limestone protoliths, and therefore variation in protolith composition is not interpreted to have strongly affected the resulting mineral assemblages.

In the southern Grant Range, stratigraphically lower Cambrian rocks are exposed, including the Pioche shale and Prospect Mountain quartzite (Fig. 3). Both of these units exhibit biotite porphyroblasts, and in one locality ~5 km south of the map area, the Pioche shale exhibits staurolite porpyhroblasts (Fryxell, 1988).

Three sequential phases of metamorphism are recorded in Cambrian and Ordovician rocks in the study area (Camilleri, 2013). The first phase accompanied mesoscale, east-vergent folding, and is defined by growth of oriented white mica porphyroblasts during development of axial-planar cleavage. The second phase involved growth of randomly oriented white mica, phlogopite, biotite, and amphibole porphyroblasts, which are interpreted as static metamorphic textures. On the basis of mineral assemblage, this stage is interpreted to have yielded the peak metamorphic conditions recorded in the Grant Range (Camilleri, 2013). This was followed by an additional stage of synkinematic metamorphism that accompanied west-vergent, mesoscale folding and thrust faulting, and is characterized by growth of oriented white mica and chlorite during development of axial-planar cleavage (Camilleri, 2013).

In the southern Grant Range, 3–10 km south of the study area, Cambrian rocks record a history of metamorphism and large-scale folding, and are intruded by the Troy granite stock (Fryxell, 1988) (Fig. 2). U-Pb zircon geochronology indicates two distinct emplacement ages for the stock (Lund et al., 2014). A boudinaged granite sill on the western margin of the stock, which pre-dates folding, yielded a Jurassic (163.3 ± 1.2 Ma) age, and undeformed granite that makes up the bulk of the pluton, and post-dates folding, yielded a Late Cretaceous age (83.7 ± 0.8 Ma) (Lund et al., 2014). A stage of static, peak metamorphism, indicated by randomly oriented porphyroblasts, is recorded in the southern Grant Range, and post-dates large-scale folding (Fryxell, 1988). The metamorphic grade of Cambrian sedimentary rocks generally decreases upsection in the southern Grant Range, but Fryxell (1988) also documented that metamorphism in Cambrian rocks dies out to the south, with distance from the granite. This suggests that Late Cretaceous magmatism may have been a primary source of heat for metamorphism.

After these observations in the southern part of the range, the stage of static, peak metamorphism in the study area in the central Grant Range has also been interpreted to have been, at least in part, contemporary with intrusion of the Late Cretaceous component of the Troy stock (Lund et al., 1993; Camilleri, 2013). This interpretation is supported by geophysical and drill hole data that suggest that the Troy pluton extends in the subsurface under the west-central Grant Range. A positive aeromagnetic anomaly, interpreted to delineate the subsurface extent of the Troy pluton (Lund et al., 1987, 1988; Blank, 1993), extends through the western part of the study area (Fig. 2). Several drill holes in Railroad Valley that fall within the area of the aeromagnetic anomaly intercept granite at depth (Fig. 2) (Lund et al., 1993; Hess et al., 2004; Long and Walker, 2015), which supports this interpretation.

In the southernmost Grant Range and farther south in the Quinn Canyon Range, east-vergent thrust faults correlated with the Central Nevada thrust belt deform Cambrian through Devonian rocks (Taylor et al., 2000) (Fig. 2). However, in the central and northern Grant Range, regionally continuous, older-over-younger relationships indicative of large-scale thrust faults have not been documented through the exposed thickness of Cambrian to Pennsylvanian rocks (Lund et al. 1993; Camilleri, 2013; Long and Walker, 2015).

Paleozoic rocks in the Grant Range are unconformably overlain by Paleogene sedimentary and volcanic rocks. 1300 m of Paleogene rocks are preserved in the study area (Long and Walker, 2015) (Fig. 3), but sections as thick as ~2000 m are reported in other parts of the range (Moores et al., 1968). In the study area, Paleogene rocks overlie Mississippian and Pennsylvanian rock units, with minimal angular discordance (Long and Walker, 2015). In addition, Eocene-Oligocene andesite, dacite, and granite dikes intruded Cambrian and Ordovician stratigraphic levels (Fig. 2) (Fryxell, 1988; Camilleri, 2013; Long and Walker, 2015). In the study area, a dacite dike yielded a crystallization age of ca. 29 Ma ($^{40}Ar/^{39}Ar$ biotite; Long and Walker, 2015), and in the southern Grant Range, a granite dike is dated at 31.7 ± 0.8 Ma (U-Pb zircon; Lund et al., 2014).

Paleozoic and Paleogene rocks in the Grant Range experienced a polyphase history of Cenozoic extension. The earliest extension was accommodated by low dip-angle, top-to-west detachment faults (Lund et al., 1993; Camilleri, 2013; Long and Walker, 2015), which initiated in the Oligocene (ca. 29–32 Ma) (Long and Walker, 2015). This was followed by one or more episodes of extension accommodated by high-angle normal faults, including Miocene to Quaternary faulting associated with formation of the Railroad Valley structural basin (Fig. 2) (Moores et al., 1968; Lund et al., 1993; Camilleri, 2013).

PEAK TEMPERATURE DATA

Structural, Stratigraphic, and Depth Context of Samples

A suite of 22 samples of Paleozoic sedimentary rocks ranging in age from Cambrian to Pennsylvanian were analyzed for the peak temperature that they experienced, using three different thermometry techniques, RSCM, vitrinite reflectance, and Rock-Eval pyrolysis. All samples were collected in the central Grant Range, within the map area of Long and Walker (2015) (Figs. 2, 5A). Samples are given structural context by projecting them to their present-day positions on the deformed cross-

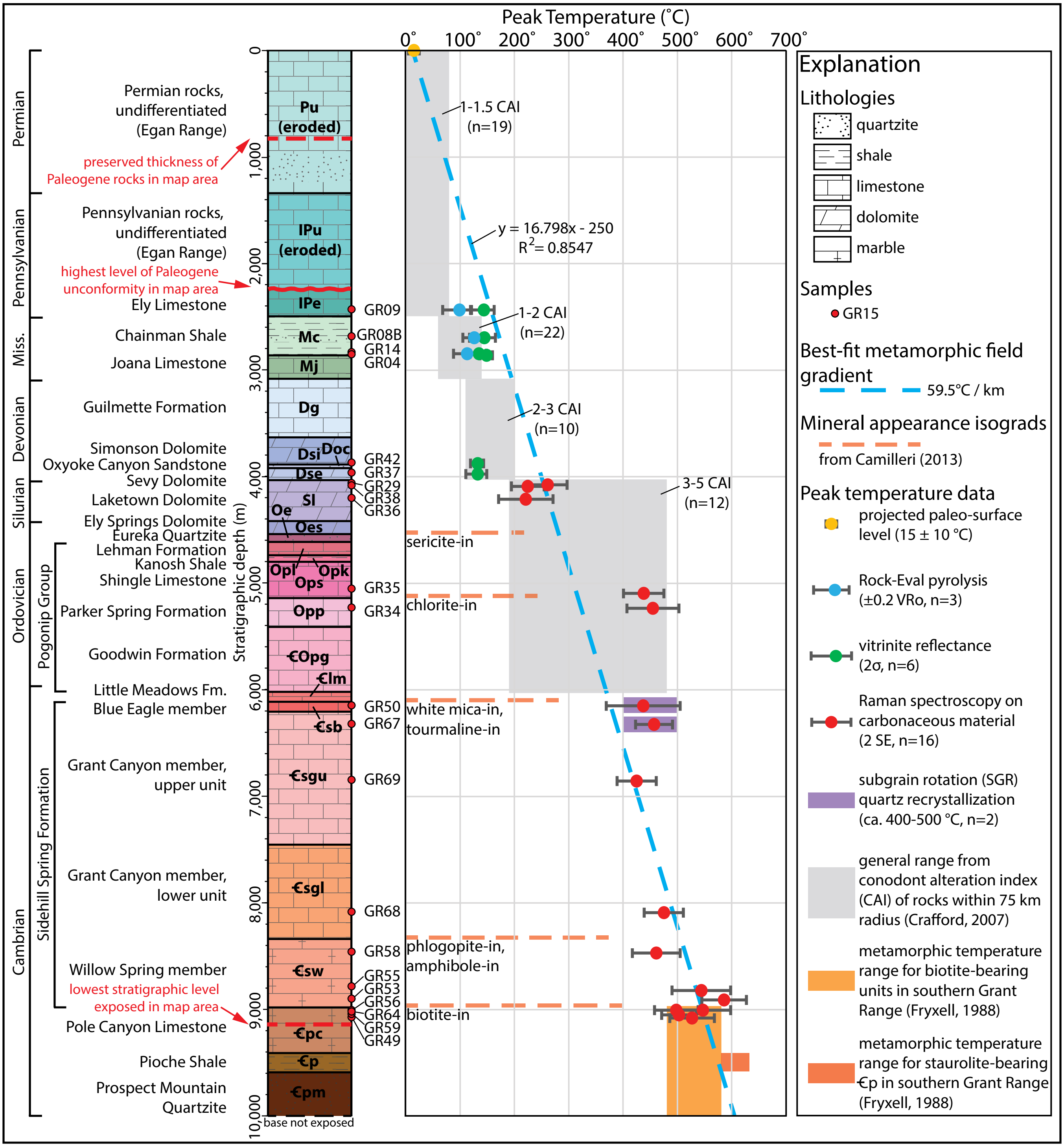

Figure 3. Stratigraphic column of Grant Range rock units, using divisions and thicknesses from Long and Walker (2015) (lithologies and estimated eroded thicknesses of Pennsylvanian and Permian rocks in the Egan Range are from Kellogg, 1963, and Brokaw and Heidrick, 1966). Column on right shows peak temperature versus stratigraphic depth below projected paleo-surface level for the 22 analyzed samples.

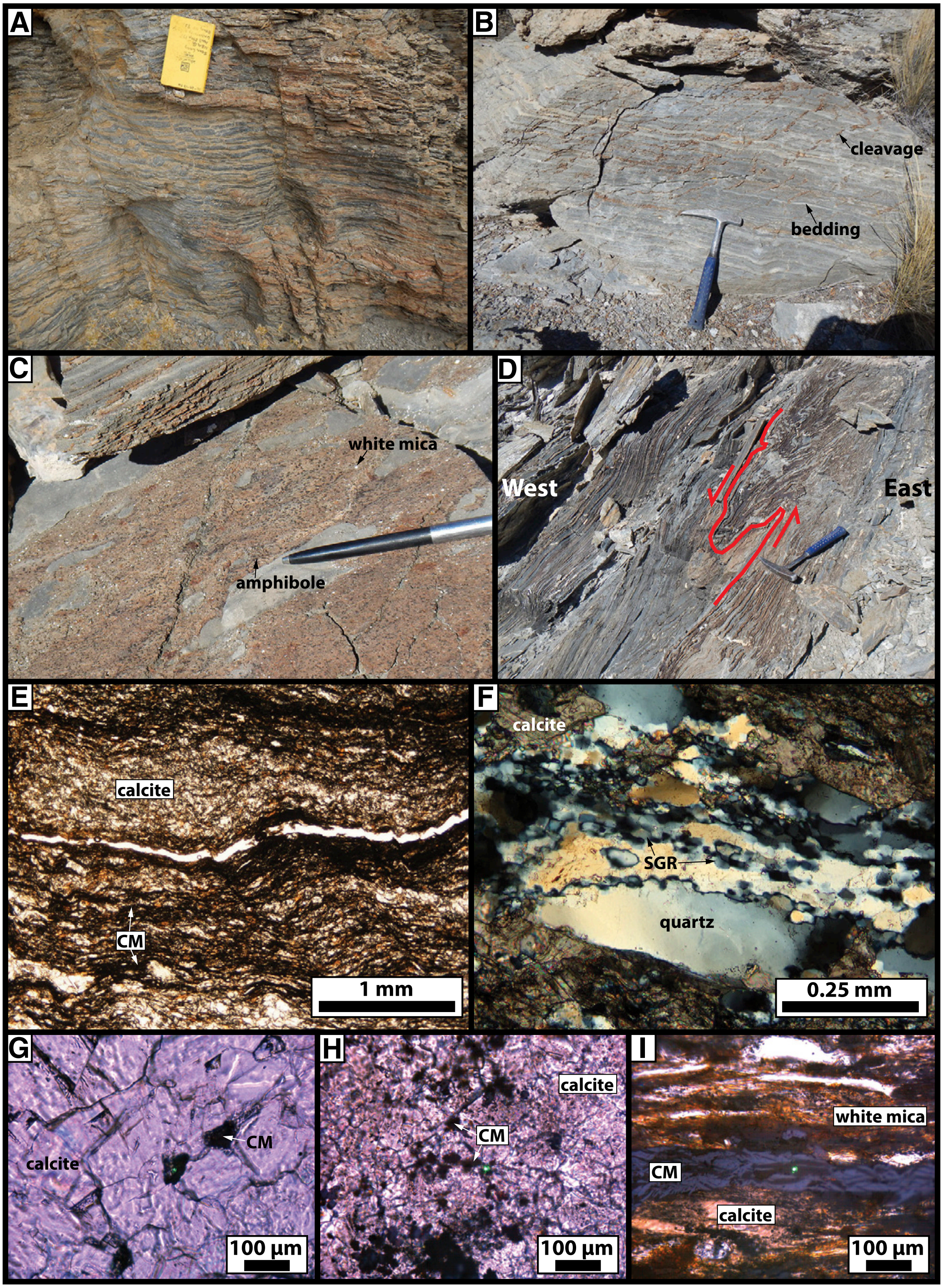

Figure 4. Photographs and photomicrographs, illustrating: (A) Thin-bedded, organic-rich limestone with phyllitic partings, characteristic of unit Ꞓsgl (refer to Fig. 3 for a guide to all unit abbreviations used in this caption). (B) Marble characteristic of unit Ꞓsw, with bedding (subhorizontal) overprinted by spaced cleavage (dipping toward left-hand side). (C) Amphibole (black) and white mica (silver) porphyroblasts within a phyllitic parting in marble of unit Ꞓsw. (D) West-vergent, mesoscale fold in phyllitic marble of unit Ꞓpc. (E) Black microlithons of carbonaceous material (CM) in marble of unit Ꞓpc (sample GR64; plane-polarized light). (F) Equigranular, polygonal quartz subgrain microstructure characteristic of subgrain rotation (SGR) recrystallization (sample GR67; cross-polarized light). (G, H, I) Representative examples of analyzed CM (G: sample GR50, spot 9; H: sample GR36, spot 3; I: sample GR55, spot 6; all taken in plane-polarized light; green spot in each photo is the Raman laser beam).

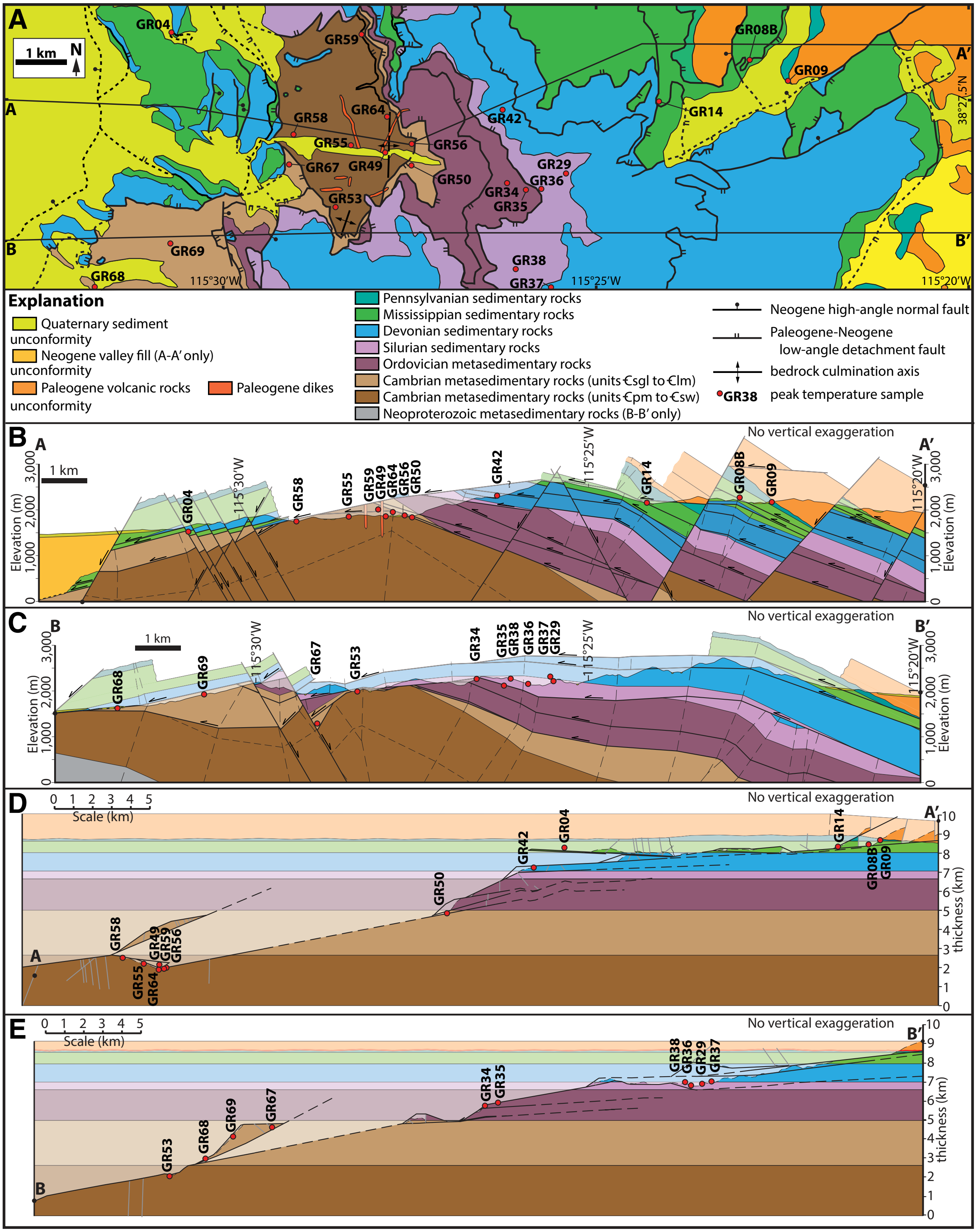

Figure 5. (A) Geologic map of the central Grant Range, generalized from Long and Walker (2015). (B, C) Cross-sections A–A′ and B–B′, generalized from Long and Walker (2015), showing present-day geometry. Translucent areas above modern erosion surface represent eroded rock. Peak temperature samples are projected along-strike to their sampled structural level. (D, E) Cross sections A–A′ and B–B′, restored for motion on Cenozoic normal and detachment faults and for the magnitude of flexural isostatic folding that accompanied extension; generalized from Long and Walker (2015). Translucent areas represent rock that has either been eroded above the modern erosion surface or translated westward off of the map area during extension. The restored positions of peak temperature samples are projected.

sections of Long and Walker (2015) (Figs. 5B, 5C). In addition, Long and Walker (2015) restored Cenozoic extension in the Grant Range by retro-deforming offset on all normal and detachment faults, and presented observations indicating that Paleozoic rocks had gentle dip magnitudes prior to extension, including documenting minimal angular discordance and structural relief across the Paleogene unconformity, and retro-deformation of the magnitude of flexural isostatic folding that accompanied extension. The samples are projected to their pre-extensional positions on the restored cross-sections of Long and Walker (2015) (Figs. 5D, 5E), which reveals that they were spread over a total east-west distance of 30–40 km prior to extension.

Based on the reconstruction of Long and Walker (2015), we assume that stratigraphic depths for the samples are approximately equivalent to pre-extensional structural depths. Samples are shown in a stratigraphic column (Fig. 3) using unit thicknesses from Long and Walker (2015), which are based on a combination of complete unit thicknesses measured in their cross sections, complete thicknesses reported in other published studies in the Grant Range (Moores et al., 1968; Fryxell, 1988; Camilleri, 2013), and minimum tectonic thicknesses for some Cambrian and Ordovician rock units. Despite using minimum thicknesses, the cumulative thicknesses of the Cambrian and Ordovician sections in the study area are comparable to nearby estimates in the White Pine and Egan Ranges (Kellogg, 1963; Moores et al., 1968), and regionally in eastern Nevada (Stewart, 1980).

The samples span a total stratigraphic thickness of 6.5 km (Fig. 3). However, assigning pre-extensional stratigraphic depths is more difficult, as an unknown thickness of rocks was eroded off of the study area prior to the Paleogene (e.g., Long, 2012). In the central Grant Range, only a few hundred meters of Pennsylvanian rocks are preserved beneath the Paleogene unconformity (Fig. 3). However, incomplete and complexly faulted sections of Pennsylvanian and Permian rocks are preserved along-strike to the north in the White Pine Range (Moores et al., 1968), which suggests that stratigraphic levels at least as high as Permian were at one time present over the study area. To the east in the Egan Range, Kellogg (1963) and Brokaw and Heidrick (1966) documented a total thickness of 2.0–2.5 km of Pennsylvanian and Permian rocks. Conodont alteration indices from Pennsylvanian and Permian rocks within a ~75 km radius of the study area are characterized by values of 1–1.5 ($n = 19$) (Crafford, 2007), which corresponds to a maximum burial temperature range of 50–80 °C (Königshof, 2003). These data indicate that Pennsylvanian and Permian rocks in the study area were not deeply buried by a thick Mesozoic section that is now eroded away (e.g., Long, 2012). On the basis of westward onlap of Triassic rocks and westward erosional truncation of Permian rocks below Triassic rocks, several studies have argued that east-central Nevada (including the study area) was a topographic high during much of the Triassic (Burchfiel et al., 1974; Collinson et al., 1976; Stewart, 1980), and therefore did not accumulate a thick section of Triassic rocks. Therefore, samples are reported on Figure 3 and Tables 1–3 at their stratigraphic depth below 2.5 km of eroded Pennsylvanian and Permian rocks, after thicknesses reported in the Egan Range (Kellogg, 1963; Brokaw and Heidrick, 1966). Based on the regional observations summarized above, these stratigraphic depths are interpreted to represent maximum permissible estimates for burial depths of rocks in the study area prior to synorogenic erosion.

RSCM Thermometry

Carbonaceous material (CM), which is derived from solid-state metamorphism of organic material (e.g., Buseck and Huang, 1985), is common in many metasedimentary rocks. Several studies have shown that the degree of structural organization of graphite bonds in CM is strongly temperature dependent, and therefore can be used as a quantitative geothermometer (e.g., Beyssac et al., 2002; Rahl et al., 2005; Aoya et al., 2010). Rahl et al. (2005) calibrated the RSCM thermometer with an uncertainty of ± 50 °C (2σ) for rocks that achieved peak temperatures between 100 and 700 °C, by measuring the height ratio (R1) and area ratio (R2) of four first-order Raman peaks (G, D1, D2, D3) in the wavenumber offset range between 1200 and 1800 cm^{-1}. Here, R1, R2, and peak temperature are determined from Equations 1, 2, and 3, respectively, of Rahl et al. (2005).

CM was analyzed from 16 samples of Cambrian, Ordovician, and Silurian rocks, with lithologies including marble, phyllite, limestone, and dolomite (Table 1; Fig. 3). Most samples contained abundant CM, which was either pres-

TABLE 1. PEAK TEMPERATURE DETERMINATIONS FROM RAMAN SPECTROSCOPY ON CARBONACEOUS MATERIAL

Sample	Map unit	Lithology	Stratigraphic depth (m)	Latitude (dd.ddddd)	Longitude (dd.ddddd)	R1		R2		Peak temperature (°C)			n
						Mean	1σ	Mean	1σ	Mean	1σ	2 SE	
GR29	Sl	dolomite	4075	38.44536	115.42425	1.466	0.224	0.721	0.043	261	42	36	13
GR38	Sl	dolomite	4090	38.44267	115.42975	1.657	0.112	0.7704	0.026	225	26	30	14
GR36	Sl	dolomite	4210	38.44267	115.42975	1.984	0.485	0.766	0.071	221	80	50	14
GR35	Ops	limestone	5095	38.44250	115.43325	0.245	0.028	0.349	0.045	438	44	37	13
GR34	Opp	limestone	5235	38.44367	115.43739	0.261	0.161	0.336	0.100	455	67	48	12
GR50	€sb	limestone	6150	38.44667	115.45867	0.190	0.098	0.335	0.111	437	95	68	10
GR67	€sgu	limestone	6325	38.44711	115.48631	0.309	0.083	0.348	0.057	457	43	34	15
GR69	€sgu	limestone	6855	38.43297	115.51264	0.463	0.131	0.414	0.070	425	46	36	14
GR68	€sgl	limestone	8090	38.42447	115.52911	0.303	0.065	0.330	0.051	475	42	36	13
GR58	€sw	marble	8470	38.45214	115.48531	0.285	0.123	0.338	0.087	461	62	44	13
GR55	€sw	phyllite	8820	38.45019	115.47253	0.139	0.055	0.221	0.079	544	69	54	10
GR53	€sw	marble	8910	38.43944	115.47581	0.117	0.043	0.176	0.054	586	46	41	11
GR56	€pc	marble	9005	38.45050	115.45886	0.161	0.101	0.224	0.100	547	84	51	15
GR64	€pc	marble	9005	38.45531	115.46428	0.205	0.045	0.283	0.061	498	53	40	13
GR59	€pc	marble	9050	38.46950	115.47017	0.176	0.046	0.270	0.043	503	35	32	14
GR49	€pc	marble	9080	38.44903	115.46467	0.211	0.064	0.257	0.067	527	57	41	14

Note: (1) R1, R2, and peak temperature values calculated using the calibration of Rahl et al. (2005). Internal variability in R1, R2, and peak temperature is indicated by 1σ uncertainty. Temperature is also reported with 2 standard errors (SE), calculated after Cooper et al. (2013), from quadratic addition of 1σ internal error and external error of ±50 °C from the Rahl et al. (2005) calibration, divided by the square root of the number of analyses (n). (2) Stratigraphic depths calculated below estimated paleo-surface level at 2.5 km above base of unit IPe, from thicknesses of Pennsylvanian and Permian rocks in the Egan Range (Kellogg, 1963; Brokaw and Heidrick, 1966).

ent within organic-rich microlithons (Figs. 4E, 4I), or as isolated patches, typically ≤50 µm in diameter (Fig. 4G, 4H). CM was analyzed in situ on polished petrographic thin sections that were cut normal to bedding. Measurements were made at the LeRoy Eyring Center for Solid State Science at Arizona State University, using a custom-built Raman spectrometer. The 532 nm laser was operated at a power of 3 mW, and was focused using a 50× ultra-long working distance Mitutoyo objective. The probed area of CM for each measurement was ~1 µm in diameter (Figs. 4G, 4I). Instrument parameters, settings, and procedures follow those outlined in Cooper et al. (2013). Where possible, the laser was focused on CM situated beneath a transparent grain (typically calcite), after procedures outlined in Beyssac et al. (2003). CM was analyzed for 120 seconds over a spectral window of 1100–2000 cm^{-1}, and typically 15 separate spots were analyzed in each sample, to allow evaluation of in-sample variation. Peak positions, heights, widths, and areas of the Raman spectra (see supplementary information for supporting data from individual analyses[1]) were determined using a custom peak fitting program written in Matlab by E. Soignard. The program allowed peak shapes to be fit by a combination of gaussian and lorentzian peaks, and any background slope to be removed by using a first-order polynomial between 1100 and 2000 cm^{-1}. Examples of representative Raman spectra for each sample are shown in Figure 6, and summary data for peak temperature determinations are shown in Table 1. Mean peak temperatures of multiple measurements are reported on Table 1, and internal uncertainty within each sample is represented by the reported 1σ error in R1, R2, and peak temperature. However, after Cooper et al. (2013), peak temperatures are reported with 2 standard errors (SE), which takes into account the external error of ± 50 °C from the Rahl et al. (2005) calibration (see footnote of Table 1). At 2 SE, typical error ranges are ± 30–50 °C (Table 1).

Resulting RSCM peak temperatures exhibit a total range between ~260 and 580 °C (Table 1; Fig. 3), and temperatures generally increase with stratigraphic depth. The three Silurian samples (GR29, GR38, GR36) yielded temperatures between ~220 and 260 °C. Seven samples from the Ordovician section and the upper and middle parts of the Cambrian section (GR35, GR34, GR50, GR67, GR69, GR68, GR58) range between ~420 and 480 °C. The lowest six samples (GR55, GR53, GR56, GR64, GR59, GR49), from Cambrian units Ꞓpc and Ꞓsw (see Figure 3 for a guide to all unit abbreviations used in the text), range between ~500 and 580 °C.

Vitrinite Reflectance Thermometry

Vitrinite reflectance, a thermal maturation parameter widely applied in the petroleum industry, can be used to estimate the peak temperature of sedimentary rocks over the range of ~50–300 °C (e.g., Barker and Pawlewicz, 1994; Mukhopadhyay, 1994). Random vitrinite reflectance, the proportion of normal incident light reflected by a polished surface of vitrinite, increases systematically with peak temperature, as the result of a series of chemical transformations that accompany hydrocarbon maturation (Mukhopadhyay, 1994).

Six samples of limestone, dolomite, and shale from Devonian, Mississippian, and Pennsylvanian rocks were analyzed for vitrinite reflectance thermometry (Table 2). Analyses were performed by Weatherford Laboratories, Inc., using procedures outlined in ASTM (2014). No primary vitrinite fragments were identified in the samples; instead, measurements of random reflectance were made on grains of solid bitumen, a vitrinite-like maceral (e.g., Landis and Castano, 1995). As few as two and as many as 30 measurements of solid bitumen reflectance (R_{SB}) were made from individual samples (supporting data in supplementary information; see footnote 1). R_{SB} values were converted into equivalent vitrinite reflectance (R_{VE}) values using the equation of Jacob (1989) (Table 2). Peak temperatures were then obtained from the mean R_{VE} value, using the calibration equation for burial heating from Barker and Pawlewicz (1994), as samples were not collected in stratigraphic continuity to allow proper thermal modeling. Error is reported at the 2σ level, which corresponds to a typical error range of ±10–25 °C. Peak temperatures determined from the six samples range between ~130 and 150 °C (Table 2; Fig. 3), and temperatures from all samples overlap within estimated error.

Rock-Eval Pyrolysis Thermometry

Rock-Eval pyrolysis, another technique widely applied in the petroleum industry to estimate the thermal maturity of organic matter, can be used to estimate the peak temperature of sedimentary rocks over the range of ~50–200 °C (e.g., Clementz, 1979; Peters, 1986). Pyrolysis involves heating of a pulverized rock sample in the absence of oxygen, in order to release and measure organic compounds (Peters, 1986). T_{max}, the oven temperature at which the maximum amount of non-volatile hydrocarbons are released, can be converted into a calculated vi-

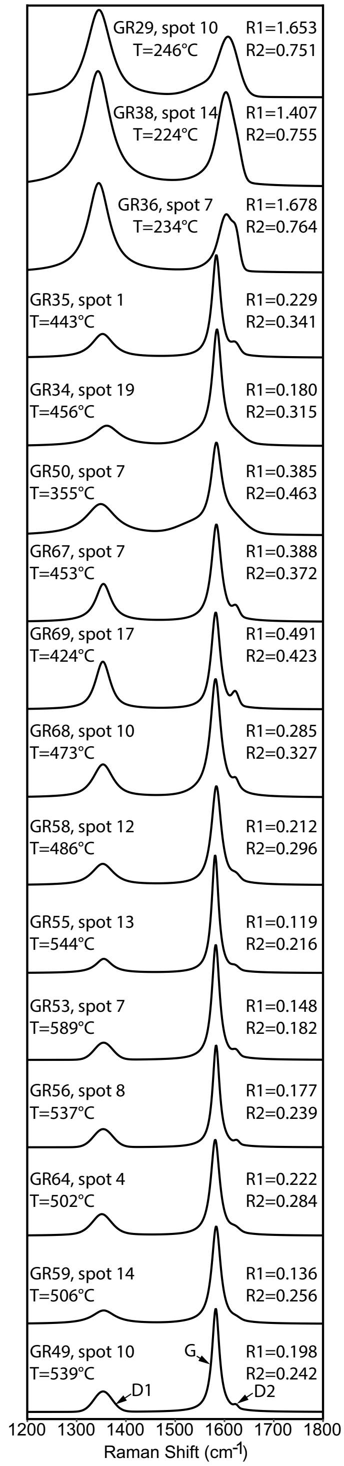

Figure 6. Examples of representative Raman spectra from each of the 16 samples analyzed for Raman spectroscopy on carbonaceous material. The positions of the graphite band (G) and defect bands (D1, D2) are shown on the bottom spectrum. Samples are stacked in stratigraphic order. Peak temperatures (T) and R1 and R2 parameters are calculated after Rahl et al. (2005). Peak center position, height, amplitude, and area are listed for individual analyses in the supplementary information (see footnote 1).

[1]GSA Data Repository Item 2016051, Tables DR1–DR3, Figure DR1 and related supporting information, is available at www.geosociety.org/pubs/ft2016.htm, or on request from editing@geosociety.org.

TABLE 2. PEAK TEMPERATURE DETERMINATIONS FROM VITRINITE REFLECTANCE

Sample	Map unit	Lithology	Stratigraphic depth (m)	Latitude (dd.ddddd)	Longitude (dd.ddddd)	Mean R_{SB} (%)	R_{SB} (1σ)	Mean R_{VE} (%)	R_{VE} (1σ)	n	T_{peak} (°C)	± 2σ error (°C)
GR09	IPe	limestone	2435	38.46167	115.37467	1.14	0.253	1.11	0.146	8	144	+19/–25
GR08B	Mc	siltstone	2695	38.46536	115.38319	1.17	0.368	1.12	0.161	2	145	+20/–27
GR14	Mc	shale	2845	38.45800	115.40414	0.95	0.150	0.99	0.090	16	135	+13/–16
GR04	Mc	limestone	2860	38.47006	115.51256	1.26	0.136	1.18	0.083	30	149	+11/–12
GR42	Dsi	dolomite	3875	38.45653	115.43808	0.91	0.117	0.96	0.071	23	132	+11/–13
GR37	Dse	dolomite	3975	38.42458	115.42819	0.91	0.196	0.96	0.112	7	132	+21/–17

Note: (1) R_{SB} was converted into R_{VE} using the equation of Jacob (1989): $R_{VE} = 0.618*R_{SB} + 0.40$. (2) T_{peak} calculated from R_{VE} values, using equation for burial heating from Barker and Pawlewicz (1994): $T_{peak} = (\ln(R_{VE}) + 1.68)/0.0124$. (3) Stratigraphic depths calculated below estimated paleo-surface level at 2.5 km above base of unit IPe, from thicknesses of Pennsylvanian and Permian rocks in the Egan Range (Kellogg, 1963; Brokaw and Heidrick, 1966). Abbreviations: R_{SB} = solid bitumen reflectance, R_{VE} = equivalent vitrinite reflectance (from Jacob, 1989), T_{peak} = peak temperature.

trinite reflectance value (cal. R_V) (Jarvie et al., 2001), and therefore can be used to estimate peak temperature.

Three samples of limestone, siltstone, and shale from Mississippian and Pennsylvanian rock units were analyzed for Rock-Eval pyrolysis (Table 3). Analyses were performed by Weatherford Laboratories, Inc., using instrument settings and procedures outlined in Clementz (1979) and Peters (1986). Additional supporting data are included in the supplementary information (see footnote 1). T_{max} was converted into cal. R_V using the equation of Jarvie et al. (2001), and peak temperature was calculated from cal. R_V using the calibration of Barker and Pawlewicz (1994). Peak temperatures for the three samples range between ~100 and 125 °C (Table 3). In the absence of a statistically meaningful procedure for calculating uncertainty, errors of ±0.2 cal. R_V were assigned, which results in a typical temperature error range of ±15–30 °C, which is comparable to the ± 2σ error range for the vitrinite reflectance analyses. Peak temperatures for all three pyrolysis samples overlap within this estimated error range (Table 3).

Peak temperature estimates for these three samples were obtained from both vitrinite reflectance and pyrolysis. Pyrolysis temperature estimates were consistently lower, by a margin of ~20–45 °C; however, temperatures from both techniques overlap within estimated error for all three samples.

Additional Peak Temperature Constraints

Three additional data sets, including quartz recrystallization microstructure, published conodont alteration indices, and published metamorphic temperature ranges based on mineral assemblage, supply semiquantitative peak temperature constraints for Paleozoic rocks in the Grant Range.

Characterization of the morphology of dynamic recrystallization of quartz in thin section allows bracketing of deformation temperature range (e.g., Stipp et al., 2002). In the study area, two samples of sandy limestone from map units Ꞓsgu (GR67) and Ꞓsb (GR50) display evidence for subgrain rotation recrystallization (Fig. 4F), which is characterized by ~0.1 mm, equigranular, polygonal quartz subgrains, and indicates deformation temperatures of ~400–500 °C (Stipp et al., 2002) (Fig. 3). This temperature range is in agreement with RSCM peak temperatures from these samples (457 ± 34 °C, 437 ± 68 °C).

Conodont alteration indices (CAI) provide semiquantitative estimates of the peak temperature that sedimentary rocks have experienced during diagenetic burial or metamorphism (e.g., Epstein et al., 1977; Königshof, 2003). Compilation of characteristic CAI values for Ordovician through Pennsylvanian sedimentary rocks within a 75 km radius of the study area, using the database of Crafford (2007), gives a general range of peak temperature versus stratigraphic level for the upper 6 km of the Paleozoic section (Fig. 3). Pennsylvanian-Permian rocks are characterized by CAI values of 1–1.5 (<50–80 °C; all CAI temperature ranges listed here are from Königshof, 2003), Mississippian rocks 1–2 (60–140 °C), Devonian rocks 2–3 (110–200 °C), and Ordovician-Silurian rocks 3–5 (190–480 °C). The CAI temperature ranges are generally in agreement with the vitrinite reflectance, Rock-Eval pyrolysis, and RSCM peak temperature determinations (Fig. 3).

In the southern Grant Range, Fryxell (1988) documented that lower Cambrian rock units, including units Ꞓpc, Ꞓp, and Ꞓpm, exhibit biotite porphyroblasts, and in one locality phyllite from unit Ꞓp exhibits staurolite porphyroblasts. Using mineral stability fields presented in Fryxell (1988), over a pressure range of 2–3 kbar, a peak temperature range of ~480–580 °C is estimated for biotite-bearing rocks, and a range of ~580–630 °C is estimated for the staurolite-bearing sample. The ~480–580 °C range is in agreement with the ~500–550 °C range of RSCM temperatures from the four biotite-bearing samples in the study area (Fig. 3).

DISCUSSION

Calculation and Interpretation of Metamorphic Field Gradient

The peak temperature samples span a 6.5 km stratigraphic thickness, and therefore can be

TABLE 3. PEAK TEMPERATURE DETERMINATIONS FROM ROCK-EVAL PYROLYSIS

Sample	Map unit	Lithology	Stratigraphic depth (m)	Latitude (dd.ddddd)	Longitude (dd.ddddd)	T_{max} (°C)	cal. R_V (%)	T_{peak} (°C)	±0.2 cal. R_V error (°C)
GR09	IPe	limestone	2435	38.46167	115.37467	433	0.63	99	+22/–31
GR08B	Mc	siltstone	2695	38.46536	115.38319	447	0.89	126	+16/–21
GR14	Mc	shale	2845	38.45800	115.40414	440	0.76	113	+19/–25

Note: (1) T_{max} = oven temperature of maximum release of non-volatile hydrocarbons. (2) cal. R_V = calculated vitrinite reflectance percentage (from Jarvie et al., 2001, conversion). (3) T_{peak} = peak temperature rock has experienced (from Barker and Pawlewicz, 1994, calibration). (4) Stratigraphic depths calculated below estimated paleo-surface level at 2.5 km above base of unit IPe, from thicknesses of Pennsylvanian and Permian rocks in the Egan Range (Kellogg, 1963; Brokaw and Heidrick, 1966).

used to estimate a metamorphic field gradient. However, interpretation of the significance of this field gradient involves several assumptions and caveats:

1. Three independent lines of evidence indicate that Paleozoic rocks in the study area were not deeply buried beyond observed regional stratigraphic depths. These include: (*a*) regional preserved sections of Pennsylvanian and Permian rocks up to 2.5 km thick (Kellogg, 1963; Brokaw and Heidrick, 1966), which consistently yield low CAI values (Crafford, 2007), and multiple studies that have argued that this region of Nevada did not accumulate a thick section of Triassic rocks (Burchfiel et al., 1974; Collinson et al., 1976; Stewart, 1980); (*b*) a lack of evidence for large-scale thrust faults and folds in the central and northern Grant Range (Lund et al. 1993; Long and Walker, 2015), which precludes significant structural burial; and (*c*) retro-deformation of Cenozoic extension in the study area, which indicates that Paleozoic rocks had low pre-extensional dip angles (Long and Walker, 2015). Therefore, pre-extensional stratigraphic depths are interpreted to approximate structural depths during peak metamorphism, indicating that the samples spanned crustal depths of 2.5–9 km. The surface level during peak metamorphism is interpreted at the top of the Permian section, and is assigned a temperature range of 15 ± 10 °C (Fig. 3).

2. All samples are assumed to have achieved peak temperature conditions at approximately the same time, during the pulse of static, peak metamorphism recorded in Cambrian and Ordovician rocks in the central and southern Grant Range (Fryxell, 1988; Camilleri, 2013). Fryxell (1988) and Camilleri (2013) both interpreted that peak metamorphism was, at least in part, synchronous with intrusion of the Late Cretaceous (ca. 84 Ma) component of the Troy granite stock. This interpretation is supported by peak Late Cretaceous (ca. 70–90 Ma) metamorphism documented across much of eastern Nevada (Miller and Gans, 1989).

3. When restored for Cenozoic extension, the positions of the peak temperature samples are spread over a total east-west distance of 30–40 km (Figs. 5D, 5E), and therefore do not represent a vertical crustal column. Therefore, the temperature gradient that these data define will not represent a true estimate of the peak geothermal gradient, but instead will be a composite estimate of peak thermal conditions obtained both laterally and vertically through the upper crust of the study area. In the absence of quantitative peak temperature data from adjacent ranges, or the ability to collect data through a vertical column in the Grant Range due to overprinting extension, the resulting metamorphic field gradient will be the most representative estimate available for the peak thermal conditions attained in the upper crust at this locality.

A best-fit line constrained by the surface temperature datapoint and the three peak temperature data sets yields a metamorphic field gradient of ~60 °C/km (Fig. 3). Using this gradient, approximate temperatures for the appearance of metamorphic minerals can be estimated, with sericite (fine-grained white mica) appearing at ~275 °C, chlorite at ~300 °C, white mica and tourmaline porphyroblasts at ~375 °C, phlogopite and amphibole porphyroblasts at ~500 °C, and biotite porphyroblasts at ~550 °C. However, the data are not perfectly linear, and between depths of 3 and 5 km, several datapoints lie below (GR42, GR37 from Devonian rocks) and above (GR35, GR34 from Ordovician rocks) the best-fit line. This could be a consequence of heterogeneous heat distribution either vertically or laterally through the crust. On the basis of the spatial proximity of metamorphic rocks to the exposed and inferred subsurface extent of the Troy stock (Fig. 2) (Fryxell, 1988; Lund et al., 1987, 1988, 1993), and the interpretation that peak metamorphism was contemporary with intrusion of the Late Cretaceous component of the stock (Fryxell, 1988; Lund et al., 1993; Camilleri, 2013), the elevated temperatures are interpreted as the result of addition of magmatic heat. Therefore, proximity to subsurface intrusive bodies is one factor that may have yielded nonlinearity in temperature versus depth.

The Grant Range in the Context of Late Cretaceous Metamorphism in the Sevier Hinterland

Late Cretaceous (ca. 70–90 Ma) granitic magmatism, metamorphism, and east-vergent, ductile contractional deformation have been documented in several areas in eastern Nevada, including the Snake Range metamorphic core complex and surrounding ranges (e.g., Miller and Gans, 1989; Lewis et al., 1999; Cooper et al., 2010), and within and east of the Ruby–East Humboldt metamorphic core complex (e.g., Hodges and Walker, 1992; Camilleri and Chamberlain, 1997; McGrew et al., 2000) (Fig. 7). While significant attention has been paid to the metamorphic conditions recorded in mid-crustal (~4–10 kbar) rocks exhumed in the footwalls of these core complexes, we emphasize here that there is also evidence for metamorphism and elevated temperatures at upper-crustal depths (≤4 kbar) preserved in several localities.

In the Ruby–East Humboldt core complex, exhumed mid-crustal rocks record a history of Late Cretaceous, upper amphibolite- to granulite-facies metamorphism, ductile thickening, magmatism, and partial melting, at peak pressure and temperature conditions of 6–10 kbar and 600–800 °C (e.g., Hodges and Walker, 1992; McGrew et al., 2000; Hallett and Spear, 2014). To the east, Paleozoic metasedimentary rocks in the Wood Hills and Pequop Mountains (Fig. 7) are interpreted to have experienced regional peak metamorphism at ca. 84 Ma, as a result of structural burial to ~4–6 kbar under the Windermere thrust sheet (Camilleri and Chamberlain, 1997). Amphibolite facies metasedimentary rocks exhumed in the footwall of the Northern Snake Range décollement (Fig. 7) were structurally buried to ~6–8 kbar, and experienced peak temperatures of ~500–650 °C, prior to exhumation (Lewis et al., 1999; Cooper et al., 2010).

In contrast, in the ranges surrounding the Northern Snake Range, Late Cretaceous peak metamorphism is also recorded within metasedimentary rocks that, prior to Cenozoic extension, restore to upper-crustal levels (Miller et al., 1988; Miller and Gans, 1989). The Deep Creek Range, Kern Mountains, Schell Creek Range, and Egan Range (Fig. 7) exhibit conformable stratigraphic successions that span the Neoproterozoic to the Triassic, encompassing the upper 12–14 km of the crust (Stewart, 1980; Miller and Gans, 1989). The deeper stratigraphic levels of these ranges, which consist of Neoproterozoic to Cambrian rocks that restore to pre-extensional depths of 8–14 km, exhibit greenschist (chlorite- and biotite-bearing) to amphibolite facies (staurolite-, garnet-, and locally andalusite- and sillimanite-bearing) mineral assemblages, which encompass an approximate total peak temperature range of 300–650 °C (Miller et al., 1988). In general, metamorphic grade increases with stratigraphic depth, and peak metamorphic field gradients, estimated from mineral stability fields and CAI data, are in many places as high as ~50 °C/km (Miller and Gans, 1989). Upper crustal metamorphic rocks in these ranges are observed over a modern (post-extensional) map area of ~135 km (N-S) by ~100 km (E-W) (Fig. 7), which indicates a broad spatial distribution of elevated upper-crustal temperatures. However, abrupt increases in metamorphic grade are also observed in proximity to Late Cretaceous plutons, defining locally high vertical and lateral temperature gradients, which indicates that the rise of granites was a primary mechanism for heat transfer to the upper crust (Barton et al., 1988; Miller et al., 1988). In addition, Cambrian and Neoproterozoic rocks exhibit synmetamorphic, east-vergent shear fabrics, which increase in intensity with depth, and are interpreted to have accommodated layer-parallel shear related to deformation in the Sevier thrust belt to the east (Miller and Gans, 1989). Peak

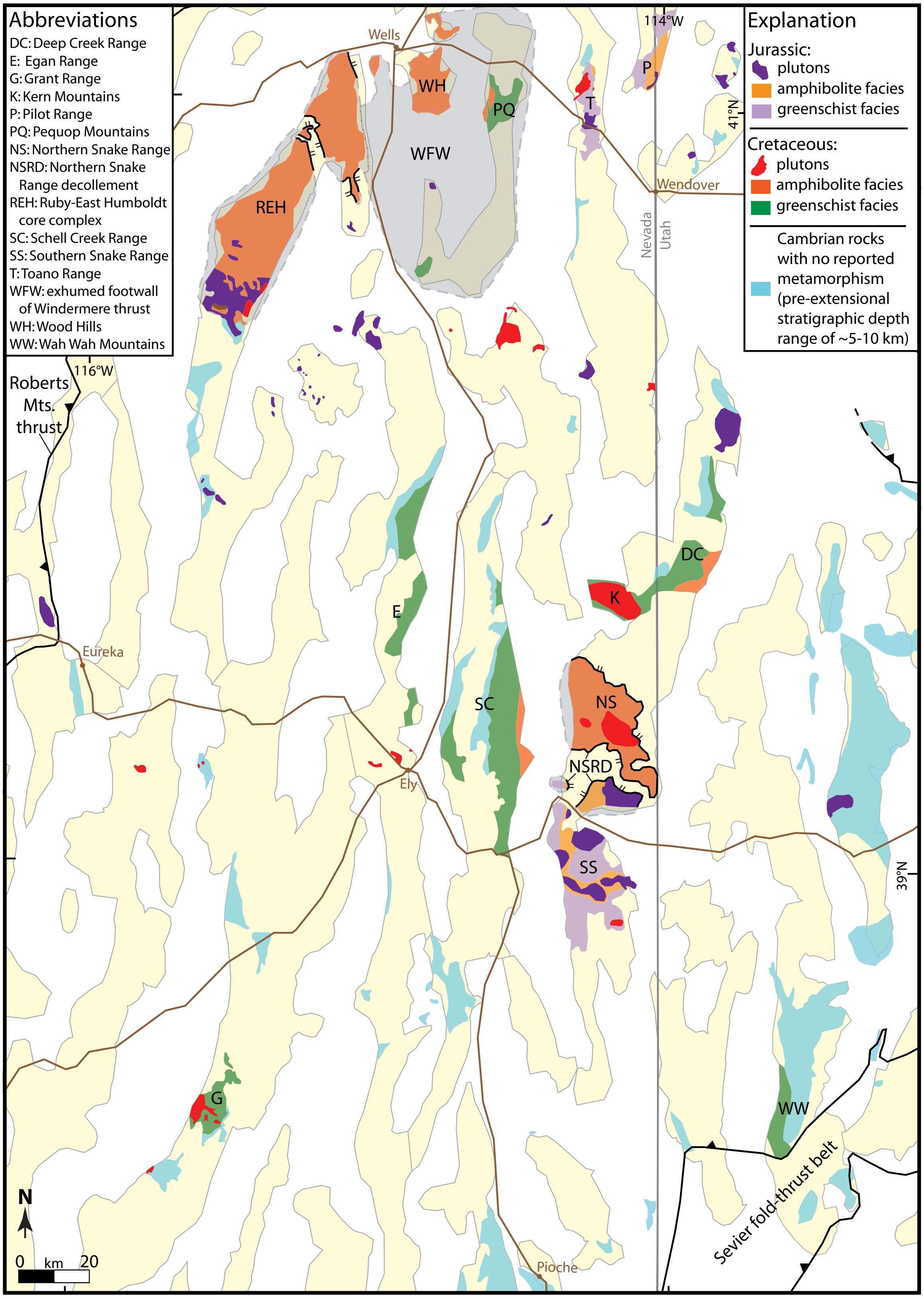

Figure 7. Map showing locations of Jurassic and Cretaceous plutons in the Sevier hinterland, and spatial distributions and grades of associated metamorphic rocks (compiled from: Stewart and Carlson, 1978; Miller et al., 1988; Miller and Gans, 1989; Miller and Hoisch, 1992, 1995; Camilleri and Chamberlain, 1997; Hintze et al., 2000; Crafford, 2007). Range and valley polygons from McQuarrie and Wernicke (2005).

metamorphism and accompanying deformation is interpreted as a protracted event that may have spanned ca. 70–90 Ma, the age range of the majority of magmatism (Miller and Gans, 1989; Barton, 1990). Late Cretaceous K-Ar and $^{40}Ar/^{39}Ar$ ages obtained from several areas suggest that the thermal regime cooled shortly after peak metamorphism (Miller et al., 1988).

Metamorphism and deformation in the Grant Range was similar in style and timing, and is interpreted here as genetically related to the Late Cretaceous, shallow-crustal metamorphism documented in the Deep Creek Range, Kern Mountains, Schell Creek Range, and Egan Range (Fig. 7). Metamorphism in the Grant Range is spatially associated with the ca. 84 Ma Troy granite stock, and was accompanied by low-magnitude, ductile contractional deformation (Camilleri, 2013), similar to observations in east-central Nevada. However, the Grant Range is exceptional in that it records metamorphism at shallower stratigraphic levels, up to the top of the Ordovician section, which corresponds to pre-extensional depths as shallow as 5 km. Similar to interpretations in east-central Nevada (Miller and Gans, 1989), the rise and emplacement of the Troy pluton is interpreted to have been the primary mechanism for heat transfer to the upper crust.

The Grant Range is separated from the larger area of upper-crustal metamorphism in east-central Nevada by ~100 km (Fig. 7). One proxy for analysis of the spatial distribution of upper-crustal heating is to look at the map distribution of exposures of Cambrian rocks, which correspond to a general, pre-extensional stratigraphic depth range of ~5–10 km (e.g., Stewart, 1980), with no reported metamorphism (Fig. 7). Quantitative peak temperature data are not available from the majority of these localities, but some published constraints do exist. Near Eureka, Long et al. (2015) obtained Paleozoic zircon fission-track and zircon (U-Th)/He ages from Cambrian quartzite, which limits the paleo-peak geothermal gradient in the upper 8 km of the crust to ~30 °C/km. Near Ely, detrital muscovite from Neoproterozoic pelitic rocks in the Duck Creek Range and Cambrian quartzite in the Schell Creek Range yielded Precambrian $^{40}Ar/^{39}Ar$ ages (Miller et al., 1988), limiting the paleo-peak geothermal gradient in the upper 8–10 km of the crust to ~35–40 °C/km. A compilation of CAI values for Cambrian and Ordovician rocks across this region of eastern Nevada (n = 125), although they display significant overall variability, are typified by values of 3–4 (n = 86) (Crafford, 2007), which corresponds to a maximum burial temperature range of ~200–300 °C (Königshof, 2003). Therefore, Cambrian rocks in the majority of these areas do not preserve evidence for anomalously high geothermal gradients, which illustrates the heterogeneous spatial distribution of upper-crustal metamorphism.

Late Cretaceous magmatism and associated metamorphism in the Sevier hinterland has been interpreted as the shallow thermal expression of an episode of lower-crustal anataxis (Barton et al., 1988; Miller and Gans, 1989; Wells and Hoisch, 2008). Causative mechanisms for lower-crustal melting are actively debated (e.g., Wells et al., 2012; Miller et al., 2012), with competing hypotheses including eastward migration of subduction-related magmatism in concert with conductive relaxation of isotherms within thickened crust (Miller and Gans, 1989), or the influx of magma, heat, and fluids following delamination of dense mantle lithosphere (Wells and Hoisch, 2008; Wells et al., 2012). Regardless of their origin, the rise of anatectic melts, to their eventual emplacement as granitic plutons at middle and upper crustal levels, provided an efficient mechanism for heat transportation, yielding metamorphism and conditions conducive for ductile deformation at shallow depths (Barton et al., 1988; Miller and Gans, 1989). The higher pluton density observed in east-central Nevada produced upper-crustal heating over a broad area (Miller et al., 1988; Barton, 1990), while the Grant Range represents a localized thermal anomaly associated with a single intrusion, which is surrounded by a large region without elevated upper-crustal temperatures.

Late Cretaceous magmatism, though spatially localized, has implications for significant thermal weakening of areas of the thickened Sevier hinterland crust. Metamorphic field gradients of 50–60 °C/km indicate that temperatures above the ~300 °C quartz crystal-plastic transition (e.g., Stipp et al., 2002) were locally achieved at depths as shallow as 5–6 km, and indicate the potential for locally attaining the ~700 °C minimum temperatures necessary for muscovite dehydration melting of pelitic rocks (e.g., Spear and Cheney, 1989) at depths possibly as shallow as 12–14 km. Experimental observations that even a small (~7%) volume percentage of partial melt can lower bulk crustal rheology by ~2 orders of magnitude (Rosenberg and Handy, 2005) imply that Late Cretaceous anataxis and associated magmatism and metamorphism could have resulted in localized but profound rheological weakening through much of the thickness of the crustal column.

Late Cretaceous magmatism and metamorphism was contemporary with late-stage shortening in the frontal Sevier thrust belt (e.g., DeCelles, 2004). Penetrative fabrics, which increase in intensity with stratigraphic depth, are observed in all of the documented areas of shallow-crustal metamorphism in eastern Nevada (Miller and Gans, 1989; Camilleri, 2013), and have been interpreted as representing the top of a diffuse zone of layer-parallel shear related to east-vergent shortening in the Sevier thrust belt (Miller and Gans, 1989). At the latitude of the large area of shallow-crustal metamorphism in east-central Nevada, ca. 88 Ma marks a slowing in crustal shortening rates in the Sevier thrust belt by a factor of ~3 (DeCelles and Coogan, 2006). Slowing of shortening rates could have been the result of the interplay of several dynamic factors, including, but not limited to, changes in interplate coupling stress, changes in décollement or wedge strength, or changing the geometry of the sedimentary basin that the thrust front migrated into. We suggest that thermal weakening of the hinterland crust may have also contributed to slowing shortening rates, by locally initiating ductile thickening at middle and lower-crustal levels. This could, at least in part, help explain the apparently disparate observations of minimal upper-crustal shortening (a few 10s of km) recorded across much of eastern and central Nevada (Taylor et al., 2000; Long, 2015) and crustal thickness estimates of ~50–60 km interpreted to have been attained across this region by the end of orogenesis (e.g., Coney and Harms, 1984; Gans, 1987; Chapman et al., 2015).

ACKNOWLEDGMENTS

This work was supported by a grant from Makoil, Inc. (Gregg Kozlowski, CEO). We are indebted to Jerome Walker for advice on the collection and interpretation of vitrinite reflectance and pyrolysis data. Conversations with Karen Lund, Sue Beard, Joan Fryxell, and Phyllis Camilleri also contributed to several ideas presented here. Thoughtful reviews from Adolph Yonkee, Karen Lund, and an anonymous reviewer greatly improved an early version of this manuscript.

REFERENCES CITED

American Society for Testing and Materials (ASTM), 2014, Standard test method for microscopical determination of the reflectance of vitrinite dispersed in sedimentary rocks, *in* Annual Book of ASTM Standards, West Conshohocken, Pennsylvania, v. D7708-14, 10 p., doi:10.1520/D7708–14.

Aoya, M., Kouketsu, Y., Endo, S., Shimizu, H., Mizukami, T., Nakamura, D., and Wallis, S., 2010, Extending the applicability of the Raman carbonaceous-material geothermometer using data from contact metamorphic rocks: Journal of Metamorphic Geology, v. 28, p. 895–914, doi:10.1111/j.1525-1314.2010.00896.x.

Barker, C.E., and Pawlewicz, M.J., 1994, Calculation of vitrinite reflectance from thermal histories and peak temperature: A comparison of methods, *in* Mukhopadhyay, P.K., and Dow, W.G., eds., Vitrinite Reflectance as a Maturity Parameter: Applications and Limitations: Washington D.C., American Chemical Society, Symposium Series v. 570, p. 216–229.

Barton, M.D., 1990, Cretaceous magmatism, metamorphism, and metallogeny in the east-central Great Basin, *in* Anderson, J.L., ed., The Nature and Origin of Cordilleran Magmatism: Geological Society of America Memoir 174, p. 283–302, doi:10.1130/MEM174-p283.

Barton, M.D., Battles, D.A., Debout, G.E., Capo, R.C., Christensen, J.N., Davis, S.R., Hanson, R.B., Michelsen, C.J., and Trim, H.E., 1988, Mesozoic contact metamorphism in the western United States, *in* Ernst, W.G., ed., Metamorphism and Crustal Evolution, Western United States, Rubey Volume VII: Englewood Cliffs, New Jersey, Prentice-Hall, p. 110–178.

Beyssac, O., Goffe, B., Chopin, C., and Rouzaud, J., 2002, Raman spectra of carbonaceous material in metasediments: A new geothermometer: Journal of Metamorphic Geology, v. 20, p. 859–871, doi:10.1046/j.1525-1314.2002.00408.x.

Beyssac, O., Goffe, B., Petitet, J.P., Froigneux, E., Moreau, M., and Rouzaud, J.N., 2003, On the characterization of disordered and heterogeneous carbonaceous materials by Raman spectroscopy: Spectrochimica Acta Part A, v. 59, p. 2267–2276, doi:10.1016/S1386-1425(03)00070-2.

Blank, H.R., 1993, Basement structure in the Railroad Valley–Grant Range region, east-central Nevada, from interpretation of potential-field anomalies, *in* Scott, R.W., Jr., Detra, P.S., and Berger, B.R., eds., Advances Related to United States and International Mineral Resources: Developing Frameworks and Exploration Technologies: U.S. Geological Survey Bulletin 2039, p. 25–30.

Brokaw, A.L., and Heidrick, T., 1966, Geologic map and sections of the Giroux Wash quadrangle, White Pine County, Nevada: U.S. Geological Survey Geology Quadrangle Map GQ-476, 1:24,000-scale.

Burchfiel, B.C., Fleck, R.J., Secor, D.T., Vincelette, R.R., and Davis, G.A., 1974, Geology of the Spring Mountains, Nevada: Geological Society of America Bulletin, v. 85, p. 1013–1022, doi:10.1130/0016-7606(1974)85<1013:GOTSMN>2.0.CO;2.

Buseck, P.R., and Huang, B.-J., 1985, Conversion of carbonaceous material to graphite during metamorphism: Geochimica et Cosmochimica Acta, v. 49, p. 2003–2016, doi:10.1016/0016-7037(85)90059-6.

Camilleri, P.A., 2013, Geologic map and structure of the west-central part of the Grant Range, Nye County, Nevada: Geological Society of America Digital Map and Chart Series DMCH014, 1 sheet, scale 1:18,000, 25 p. text, doi:10.1130/2013.DMCH014.

Camilleri, P.A., and Chamberlain, K.R., 1997, Mesozoic tectonics and metamorphism in the Pequop Mountains and Wood Hills region, northeast Nevada: Implications for the architecture and evolution of the Sevier orogeny: Geological Society of America Bulletin, v. 109, p. 74–94, doi:10.1130/0016-7606(1997)109<0074:MTAMIT>2.3.CO;2.

Cassel, E.J., Breecker, D.O., Henry, C.D., Larson, T.E., and Stockli, D.F., 2014, Profile of a paleo-orogen: high topography across the present-day Basin and Range from 40 to 23 Ma: Geology, v. 42, p. 1007–1010, doi:10.1130/G35924.1.

Chapman, J.B., Ducea, M.N., DeCelles, P.G., and Profeta, L., 2015, Tracking changes in crustal thickness during orogenic evolution with Sr/Y: An example from the North American Cordillera: Geology, v. 43, p. 919–922, doi:10.1130/G36996.1.

Clementz, D.M., 1979, Effect of oil and bitumen saturation on source-rock pyrolysis: The American Association of Petroleum Geologists Bulletin, v. 63, p. 2227–2232.

Colgan, J.P., and Henry, C.D., 2009, Rapid middle Miocene collapse of the Sevier orogenic plateau in north-central Nevada: International Geology Review, v. 51, p. 920–961, doi:10.1080/00206810903056731.

Collinson, J.W., Kendall, C.G., and Marcantel, J.B., 1976, Permian-Triassic boundary in eastern Nevada and west-central Utah: Geological Society of America Bulletin, v. 87, p. 821–824, doi:10.1130/0016-7606(1976)87<821:PBIENA>2.0.CO;2.

Coney, P.J., and Harms, T.J., 1984, Cordilleran metamorphic core complexes: Cenozoic extensional relics of Mesozoic compression: Geology, v. 12, p. 550–554, doi:10.1130/0091-7613(1984)12<550:CMCCCE>2.0.CO;2.

Cooper, F.J., Platt, J.P., Anczkiewicz, R., and Whitehouse, M.J., 2010, Footwall dip of a core complex detachment fault: thermobarometric constraints from the northern Snake Range (Basin and Range, USA): Journal of Metamorphic Geology, v. 28, p. 997–1020, doi:10.1111/j.1525-1314.2010.00907.x.

Cooper, F.J., Hodges, K.V., and Adams, B.A., 2013, Metamorphic constraints on the character and displacement of the South Tibetan fault system, central Bhutanese Himalaya: Lithosphere, v. 5, p. 67–81, doi:10.1130/L221.1.

Crafford, A.E.J., 2007, Geologic Map of Nevada: U.S. Geological Survey Data Series, v. 249, 1 CD-ROM, 46 p.

Cruz-Uribe, A.M., Hoisch, T.D., Wells, M.L., Vervoort, J.D., and Mazdab, F.K., 2015, Linking thermodynamic modelling, Lu-Hf geochronology and trace elements in garnet: new P-T-t paths from the Sevier hinterland: Journal of Metamorphic Geology, v. 33, p. 763–781, doi:10.1111/jmg.12151.

Currie, B.S., 2002, Structural configuration of the Early Cretaceous Cordilleran foreland-basin system and Sevier thrust belt, Utah and Colorado: The Journal of Geology, v. 110, p. 697–718, doi:10.1086/342626.

DeCelles, P.G., 2004, Late Jurassic to Eocene evolution of the Cordilleran thrust belt and foreland basin system, western U.S.A: American Journal of Science, v. 304, p. 105–168, doi:10.2475/ajs.304.2.105.

DeCelles, P.G., and Coogan, J.C., 2006, Regional structure and kinematic history of the Sevier fold-and-thrust belt, central Utah: Geological Society of America Bulletin, v. 118, p. 841–864, doi:10.1130/B25759.1.

Dickinson, W.R., 2002, The Basin and Range province as a composite extensional domain: International Geology Review, v. 44, p. 1–38, doi:10.2747/0020-6814.44.1.1.

Druschke, P., Hanson, A.D., and Wells, M.L., 2009, Structural, stratigraphic, and geochronologic evidence for extension predating Palaeogene volcanism in the Sevier hinterland, east-central Nevada: International Geology Review, v. 51, p. 743–775, doi:10.1080/00206810902917941.

Epstein, A.G., Epstein, J.B., and Harris, L.D., 1977, Conodont color alteration—An index to organic metamorphism: U.S. Geological Survey Professional Paper 995, 27 p.

Fryxell, J.E., 1988, Geologic map and description of stratigraphy and structure of the west-central Grant Range, Nye County, Nevada: Geological Society of America Map and Chart Series MCH064, 16 p. text.

Gans, P.B., 1987, An open-system, two-layer crustal stretching model for the eastern Great Basin: Tectonics, v. 6, p. 1–12, doi:10.1029/TC006i001p00001.

Gans, P.B., Seedorff, E., Fahey, P.L., Hasler, R.W., Maher, D.J., Jeanne, R.A., and Shaver, S.A., 2001, Rapid Eocene extension in the Robinson district, White Pine County, Nevada: Constraints from ^{40}Ar/^{39}Ar dating: Geology, v. 29, p. 475–487, doi:10.1130/0091-7613(2001)029<0475:REEITR>2.0.CO;2.

Hallett, B.W., and Spear, F.S., 2014, The P-T History of anatectic pelites of the northern East Humboldt Range, Nevada: evidence for tectonic loading, decompression, and anataxis: Journal of Petrology, v. 55, p. 3–36, doi:10.1093/petrology/egt057.

Hess, R.H., Fitch, S.P., and Warren, S.N., 2004, Nevada oil and gas well database: Nevada Bureau of Mines and Geology Open-File Report 04-1.

Hintze, L.F., Willis, G.C., Laes, D.Y.M., Sprinkel, D.A., and Brown, K.D., 2000, Digital geologic map of Utah: Utah Geological Survey Map 179DM, scale 1:500,000.

Hodges, K.V., and Walker, J.D., 1992, Extension in the Cretaceous Sevier orogen, North American Cordillera: Geological Society of America Bulletin, v. 104, p. 560–569, doi:10.1130/0016-7606(1992)104<0560:EITCSO>2.3.CO;2.

Hoisch, T.D., Wells, M.L., Beyene, M.A., Styger, S., and Vervoort, J.D., 2014, Jurassic Barrovian metamorphism in a western U.S. Cordilleran metamorphic core complex, Funeral Mountains, California: Geology, v. 42, p. 399–402, doi:10.1130/G35352.1.

Humphreys, E.D., 1995, Post-Laramide removal of the Farallon slab, western United States: Geology, v. 23, p. 987–990, doi:10.1130/0091-7613(1995)023<0987:PLROTF>2.3.CO;2.

Jacob, H., 1989, Classification, structure, genesis and practical importance of natural solid oil bitumen ("migrabitumen"): International Journal of Coal Geology, v. 11, p. 65–79, doi:10.1016/0166-5162(89)90113-4.

Jarvie, D.M., Claxton, B.L., Henk, F., and Breyer, J.T., 2001, Oil and shale gas from the Barnett Shale, Ft. Worth Basin, Texas: American Association of Petroleum Geologists Bulletin, v. 85, supplement, p. A100.

Jordan, T.E., 1981, Thrust loads and foreland basin evolution, Cretaceous, western United States: American Association of Petroleum Geologists Bulletin, v. 65, p. 2506–2520.

Kellogg, H.E., 1963, Paleozoic stratigraphy of the Southern Egan Range, Nevada: Geological Society of America Bulletin, v. 74, p. 685–708, doi:10.1130/0016-7606(1963)74[685:PSOTSE]2.0.CO;2.

Kelly, E.D., Hoisch, T.D., Wells, M.L., Vervoort, J.D., and Beyene, M.A., 2015, An Early Cretaceous garnet pressure-temperature path recording synconvergent burial and exhumation from the hinterland of the Sevier orogenic belt, Albion Mountains, Idaho: Contributions to Mineralogy and Petrology, v. 170, n. 20, 22 p., doi:10.1007/s00410-015-1171-2.

Kleinhampl, F.J., and Ziony, J.L., 1985, Geology of northern Nye County, Nevada: Nevada Bureau of Mines and Geology Bulletin 99A, 171 p.

Königshof, P., 2003, Conodont deformation patterns and textural alteration in Paleozoic conodonts: examples from Germany and France: Paleobiodiversity and Paleoenvironments, v. 83, p. 149–156, doi: 10.1007/BF03043310.

Landis, C.R., and Castano, J.R., 1995, Maturation and bulk chemical properties of a suite of solid hydrocarbons: Organic Geochemistry, v. 22, p. 137–149, doi:10.1016/0146-6380(95)90013-6.

Lewis, C.J., Wernicke, B.P., Selverstone, J., and Bartley, J.M., 1999, Deep burial of the footwall of the northern Snake Range decollement, Nevada: Geological Society of America Bulletin, v. 111, p. 39–51, doi:10.1130/0016-7606(1999)111<0039:DBOTFO>2.3.CO;2.

Long, S.P., 2012, Magnitudes and spatial patterns of erosional exhumation in the Sevier hinterland, eastern Nevada and western Utah, U.S.A.: Insights from a Paleogene paleogeologic map: Geosphere, v. 8, p. 881–901, doi:10.1130/GES00783.1.

Long, S.P., 2014, Preliminary geologic map of Heath Canyon, central Grant Range, Nye County, Nevada: Nevada Bureau of Mines and Geology Open-File Report 14-6, 1:24,000-scale, 4 p.

Long, S.P., 2015, An upper-crustal fold province in the hinterland of the Sevier orogenic belt, eastern Nevada, U.S.A.: a Cordilleran Valley and Ridge in the Basin and Range: Geosphere, v. 11, p. 404–424, doi:10.1130/GES01102.1.

Long, S.P., and Walker, J.P., 2015, Geometry and kinematics of the Grant Range brittle detachment system, eastern Nevada, U.S.A.: an end-member style of upper-crustal extension: Tectonics, v. 34, 26 p., doi: 10.1002/2015TC003918.

Long, S.P., Henry, C.D., Muntean, J.L., Edmondo, G.P., and Cassel, E.J., 2014, Early Cretaceous construction of a structural culmination, Eureka, Nevada, U.S.A.: implications for out-of-sequence deformation in the Sevier hinterland: Geosphere, v. 10, p. 564–584, doi:10.1130/GES00997.1.

Long, S.P., Thomson, S.N., Reiners, P.W., and Di Fiori, R.V., 2015, Synorogenic extension localized by upper-crustal thickening: an example from the Late Cretaceous Nevadaplano: Geology, v. 43, p. 351–354, doi:10.1130/G36431.1.

Lund, K., Nash, J.T., Beard, L.S., Blank, H.R., Jr., and Tuftin, S.E., 1987, Mineral Resources of the Blue Eagle Wilderness Study Area, Nye County, Nevada: U.S. Geological Survey Bulletin 1731-D, 19 p.

Lund, K., Beard, L.S., Blank, H.R., Jr., Hofstra, A.H., and Hamilton, M.M., 1988, Mineral Resources of the Riordans Well Wilderness Study Area, Nye County, Nevada: U.S. Geological Survey Bulletin 1731-H, 16 p.

Lund, K., Beard, S.L., and Perry, W.J., 1993, Relation between extensional geometry of the northern Grant Range and oil occurrences in Railroad Valley, east-central Nevada: The American Association of Petroleum Geologists Bulletin, v. 77, p. 945–962, doi:10.1306/BDFF8DA8-1718-11D7-8645000102C1865D.

Lund, K., Beard, S.L., and Colgan, J.P., 2014, Shrimp U-Pb dating of zircon reveals Oligocene, Late Cretaceous, and Late Jurassic ages in Troy granite, east-central Nevada: Geological Society of America Abstracts with Programs, v. 46, no. 5, p. 30.

McGrew, A.J., Peters, M.T., and Wright, J.E., 2000, Thermobarometric constraints on the tectonothermal evolution of the East Humboldt Range metamorphic core complex, Nevada: Geological Society of America Bulletin, v. 112, p. 45–60, doi:10.1130/0016-7606(2000)112<45:TCOTTE>2.0.CO;2.

McQuarrie, N., and Wernicke, B.P., 2005, An animated tectonic reconstruction of southwestern North America since 36 Ma: Geosphere, v. 1, p. 147–172, doi:10.1130/GES00016.1.

Miller, D.M., and Hoisch, T.D., 1992, Mesozoic structure, metamorphism, and magmatism in the Pilot and Toano

Ranges, *in* Wilson, J.R., ed., Field guide to geologic excursions in Utah and adjacent areas of Nevada, Idaho, and Wyoming: Utah Geological Survey Miscellaneous Publication, v. 92-3, p. 79–92.
Miller, D.M., and Hoisch, T.D., 1995, Jurassic tectonics of northeastern Nevada and northwestern Utah from the perspective of barometric studies: Geological Society of America Special Paper 299, p. 267–294, doi:10.1130/SPE299-p267.
Miller, E.L., and Gans, P.B., 1989, Cretaceous crustal structure and metamorphism in the hinterland of the Sevier thrust belt, western U.S. Cordillera: Geology, v. 17, p. 59–62, doi:10.1130/0091-7613(1989)017<0059:CCSAMI>2.3.CO;2.
Miller, E.L., Gans, P.B., Wright, J.E., and Sutter, J.F., 1988, Metamorphic history of the east central Basin and Range Province: Tectonic setting and relationship to magmatism, *in* Ernst, W.G., ed., Metamorphism and Crustal Evolution, Western United States: Englewood Cliffs, New Jersey, Prentice-Hall, Rubey Volume VII, p. 649–682.
Miller, E.L., Konstantinou, A., and Strickland, A., 2012, Comment on "Geodynamics of synconvergent extension and tectonic mode switching: Constraints from the Sevier-Laramide orogen" by Michael L. Wells et al. Tectonics, v. 31, TC4015, doi:10.1029/2012TC003103.
Moores, E.M., Scott, R.B., and Lumsden, W.W., 1968, Tertiary tectonics of the White Pine–Grant Range, east-central Nevada, and some regional implications: Geological Society of America Bulletin, v. 79, p. 1703–1726, doi:10.1130/0016-7606(1968)79[1703:TTOTWP]2.0.CO;2.
Mukhopadhyay, P., 1994, Vitrinite reflectance as a maturity parameter: Petrographic and molecular characterization and its application to basin modeling, *in* Mukhopadhyay, P., and Dow, W.G., eds., Vitrinite Reflectance as a Maturity Parameter: Applications and Limitations: Washington D.C., American Chemical Society, Symposium Series v. 570, p. 1–24.
Peters, K.E., 1986, Guidelines for evaluating petroleum source rock using programmed pyrolysis: The American Association of Petroleum Geologists Bulletin, v. 70, p. 318–329.
Rahl, J.M., Anderson, K.M., Brandon, M.T., and Fassoulas, C., 2005, Raman spectroscopic carbonaceous material thermometry of low-grade metamorphic rocks: Calibration and application to tectonic exhumation in Crete, Greece: Earth and Planetary Science Letters, v. 240, p. 339–354, doi:10.1016/j.epsl.2005.09.055.
Rosenberg, C.L., and Handy, M.R., 2005, Experimental deformation of partially-melted granite revisited: implications for the continental crust: Journal of Metamorphic Geology, v. 23, p. 19–28, doi:10.1111/j.1525-1314.2005.00555.x.
Snell, K.E., Koch, P.L., Druschke, P., Foreman, B.Z., and Eiler, J.M., 2014, High elevation of the 'Nevadaplano' during the Late Cretaceous: Earth and Planetary Science Letters, v. 386, p. 52–63, doi: 10.1016 /j.epsl. 2013.10.046.
Spear, F.S., and Cheney, J.T., 1989, A petrogenetic grid for pelitic schists: Contributions to Mineralogy and Petrology, v. 101, p. 149–164, doi:10.1007/BF00375302.
Stewart, J.H., 1980, Geology of Nevada: a discussion to accompany the Geologic Map of Nevada: Reno, Nevada, Nevada Bureau of Mines and Geology Special Publication, v. 4, 136 p.
Stewart, J.H., and Carlson, J.E., 1978, Geologic map of Nevada: U.S. Geological Survey in collaboration with the Nevada Bureau of Mines and Geology, 1 plate, scale 1:500,000.
Stipp, M., Stunitz, H., Heilbronner, R., and Schmid, S.M., 2002, The eastern Tonale fault zone: a 'natural laboratory' for crystal plastic deformation over a temperature range from 250° to 700°C: Journal of Structural Geology, v. 24, p. 1861–1884, doi:10.1016/S0191-8141(02)00035-4.
Taylor, W.J., Bartley, J.M., Martin, M.W., Geissman, J.W., Walker, J.D., Armstrong, P.A., and Fryxell, J.E., 2000, Relations between hinterland and foreland shortening: Sevier orogeny, central North American Cordillera: Tectonics, v. 19, p. 1124–1143, doi:10.1029/1999TC001141.
Wells, M.L., and Hoisch, T.D., 2008, The role of mantle delamination in widespread Late Cretaceous extension and magmatism in the Cordilleran orogen, western United States: Geological Society of America Bulletin, v. 120, p. 515–530, doi:10.1130/B26006.1.
Wells, M.L., Hoisch, T.D., Cruz-Aribe, A.M., and Vervoort, J.D., 2012, Geodynamics of synconvergent extension and tectonic mode switching: Constraints from the Sevier-Laramide orogeny: Tectonics, v. 31, TC1002, 20 p., doi:10.1029/2011TC002913.

MANUSCRIPT RECEIVED 12 OCTOBER 2015
REVISED MANUSCRIPT RECEIVED 31 DECEMBER 2015
MANUSCRIPT ACCEPTED 11 JANUARY 2016

Printed in the USA